Materials Science and Engineering B 178 (2013) 1285–1295

Contents lists available at ScienceDirect

Materials Science and Engineering B

journal homepage: www.elsevier.com/locate/mseb

Electromagnetic metamaterials

Raimond Grimberg*

Nondestructive Testing Department, National Institute of Research and Development for Technical Physics, 47 D. Mangeron Boulevard, Iasi 700050, Romania

ARTICLE INFO

Article history:
Received 29 October 2012
Received in revised form 29 January 2013
Accepted 11 March 2013
Available online 16 April 2013

Keywords:
Electromagnetic metamaterials
Negative permittivity
Negative permeability
Swiss roll
Nondestructive evaluation
Sensors

ABSTRACT

This paper proposes a review of electromagnetic metamaterials based on the idea that these are composite materials, their properties depending of the type and dimensions of the structural elements as well as the dimensions of unit cell. From the multitude of structural elements, only few that could present negative permittivity and negative or very high permeability in the range of radio and microwave frequency were chosen. The method of determination for the constitutive parameters (μ_{eff} and ε_{eff}) of metamaterials based on the *S* parameters or transmission and reflection coefficients is presented. Moreover, some applications of metamaterials are described, the attention being focused on perfect lenses and novel structures, namely conical Swiss rolls, electromagnetic cloaks and sensors for nondestructive evaluation of materials. Given that the spatial resolution of these sensors can be substantially improved in comparison to classical sensors, the metamaterial lenses are used for the manipulation of evanescent waves.

1. Introduction

One of the remarkable aspects of the human civilizational development is the intention to create or construct something that is not available in natural surroundings [1]. Initially, people attempted to rearrange objects around them. Then, they started to modify the shape and structure of the objects, to split them into parts, to combine different ones, the humanity reaching then to make their first tools. Useful substances started to be extracted from natural resources, the complexity of procedures increasing together with the aim of obtaining materials with specified properties. Further on, the materials have been synthetized due to the development of manipulation methods at molecular and atomic levels respectively. Furthermore, spectacular properties of materials can be also obtained by manipulation of certain structures, various composites being thus created.

Somehow, every material is a composite, even if the individual components are atoms and molecules [2]. Therefore, it is only a small step to replace the atoms of the original concept with structures on a larger scale and to pass from materials to metamaterials.

Metamaterials are an arrangement of artificial structural elements designed to achieve advantageous and unusual properties. A detailed consideration of the terminology is presented in [3].

In most cases, metamaterials consists of a periodical lattice of identical elements (or sets of elements), being analogy to crystals, as showed in Fig. 1. The constitutive elements of a metamaterial are named metaatoms or metamolecules. Through the metaatoms presented in Fig. 1, detailed analyzed in the paper, we can identify wire meshes, splitter ring resonators, conical Swiss rolls, Swiss rolls, further development of this fascinating domain allowing other types of constitutive elements.

An amorphous substance consists of random or irregular arrangement of artificial structural elements. We shall consider periodic structures defined by a unit cell of characteristic dimensions *a*, defined by [2]

$$a \ll \lambda$$

where λ is the wavelength of incident electromagnetic waves.

In this limit an effective permittivity and permeability is a valid concept.

Metamaterials have various applications, starting from perfect lenses [4–6] and invisible cloaks [7,8], antennas [9,10] and different types of sensors [11–13].

This paper aims to be a review in the domain of electromagnetic metamaterials, focusing on the state of the art in sensing technologies using metamaterials.

2. Metamaterials structural elements

Nowadays, a multitude of metamaterials structural elements types are known, giving special electromagnetic properties. In principle, the structural elements of metamaterials might be classified into two categories: those with negative dielectric permittivity and, in a certain frequency range, those with negative magnetic

* Tel.: +40 232430680.
E-mail address: grimberg@phys-iasi.ro

0921-5107/$ – see front matter © 2013 Elsevier B.V. All rights reserved.
http://dx.doi.org/10.1016/j.mseb.2013.03.022

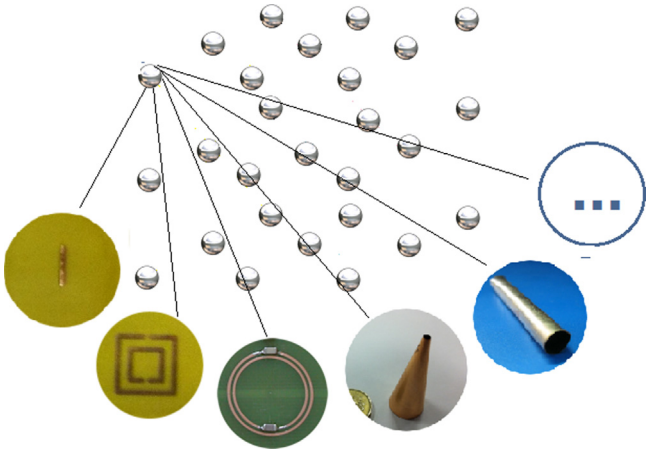

Fig. 1. Metamaterial concept.

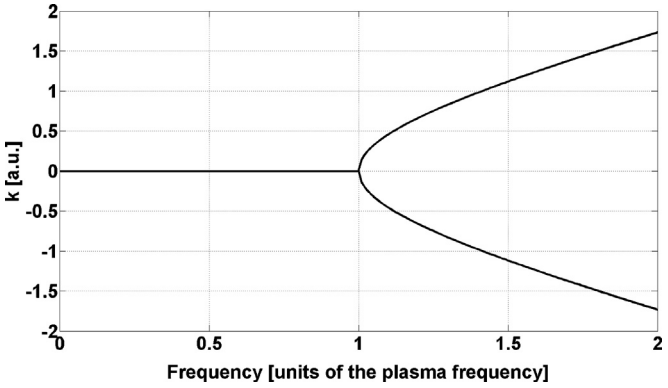

Fig. 2. Dispersion equation for light in an ideal metal.

permeability or very high magnetic permeability, although the elements are made from paramagnetic materials.

2.1. Materials with negative permittivity

2.1.1. Metals and plasmons at optical frequencies

At optical frequencies, many metals have a negative dielectric permittivity when the conductive electrons in metals can be assumed reasonably free. It is the plasma-like behavior that is responsible for a negative dielectric permittivity at frequencies smaller than the plasma frequency. The dielectric permittivity of the metals is

$$\varepsilon(\omega) = 1 - \frac{\omega_p^2}{\omega(\omega + j\gamma)} \tag{1}$$

where ω_p is the bulk frequency, γ is the damping constant and ω is the angular frequency of the incident planar electromagnetic wave. The bulk plasma frequency depends on the electron density, n, the electron mass, m_e and charge e respectively

$$\omega_p^2 = \frac{ne^2}{\varepsilon_0 m_e} \tag{2}$$

This is the Drude theory for the dispersion characteristics of a plasma [14], the dispersion equation gaining the form

$$k = \frac{\omega}{c}\sqrt{1 - \frac{\omega_p^2}{\omega^2}} \tag{3}$$

and is represented in Fig. 2.

Below the plasma frequency, in a metal only evanescent modes (with imaginary wave vector) can exist. Two degenerate modes emerge at the plasma frequency as shown in Fig. 2.

Consider the interface between an ideal metal (characterized by ε_m) and a dielectric (ε_d), for example vacuum, "illuminated" with an electromagnetic wave, p polarized as is presented in Fig. 3. Here, the frequency has been chosen so that $\varepsilon_m < 0$ and $\varepsilon_d \geq 1$ ($\varepsilon_d = 1$ for vacuum), Fig. 3.

The fields between two media, as is presented in Fig. 3, can be written

$$\begin{aligned} \bar{E}_d &= \bar{E}_0 \exp(j(k_x x + k_y y - \omega t) - K_{z+} z), \quad z > 0 \\ \bar{E}_m &= \bar{E}_0 \exp(j(k_x x + k_y y - \omega t) - K_{z-} z), \quad z < 0 \end{aligned} \tag{4}$$

Using the continuity equations for the tangential components of the electrical fields at the interface, it is obtained

$$k_x^2 + k_y^2 - K_{z+}^2 = \frac{\varepsilon_d \mu_0 \omega^2}{c^2} \qquad k_x^2 + k_y^2 - K_{z-}^2 = \frac{\varepsilon_m \mu_0 \omega^2}{c^2} \qquad \text{or} \quad \frac{K_{z+}}{\varepsilon_d} + \frac{K_{z-}}{\varepsilon_m} = 0$$

There are collective excitations of electrons with the charges displaced parallel to the real part of the wave vector. Therefore, there is a mode with the amplitude of the longitudinal component of the fields decaying exponentially between the metal and the dielectric. Hence, this charge density wave lines on the surface of the metal and is called a surface plasmons, characterized by the dispersion equation

$$k_x = \frac{\omega}{c}\left(\frac{\varepsilon_m \varepsilon_d}{\varepsilon_m + \varepsilon_d}\right)^{1/2} \tag{5}$$

for a metal with $\varepsilon_m(\omega)$, given by Eq. (1) and setting $\varepsilon_d = 1$ for vacuum, $k_x > \omega/c$ for the surface plasmons [15]. Hence it will not be possible to excite the surface plasmons on a perfectly flat surface using propagating modes of light. For the surface plasmons excitation are necessary some mechanisms such as the surface roughness, a metallic strip grating structure or a dielectric coupler to vacuum such as a prism or a hemisphere [16].

2.1.2. Wire-mesh structure

Metal-dielectric structures have long been studied for their rich electrodynamics response [2]. It has been demonstrated in [16] that the metallic wire-mesh structures have low frequency stop band from zero frequency up to the cut-off frequency which can be attributed to the motion of electrons in metal wires. This

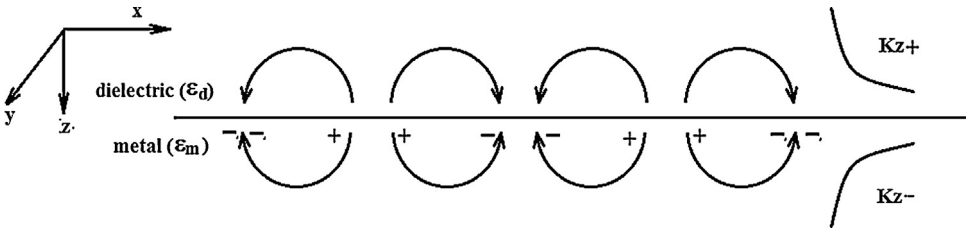

Fig. 3. Surface plasmon on an interface between a dielectric ($\varepsilon_d > 0$) and a metal ($\varepsilon_m < 0$).

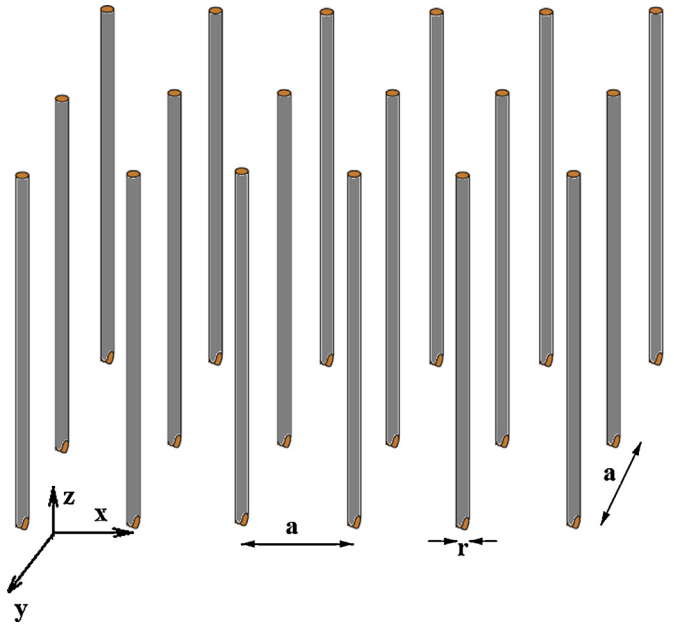

Fig. 4. An array of infinitely long thin metal wires of radius r and a lattice period a.

structural element consists of very thin wires structures on truly sub-wavelength scale, as is presented in Fig. 4

The electric field is considered to be applied parallel to the wires and $\lambda \gg r$, a. The electrons are confined to move within the wires only, which reduces the effective electron density [2].

The plasmons frequency, from the longitudinal plasmonic mode for the system is [16]

$$\omega_p = \frac{2\pi c^2}{a^2 \ln(a/r)} \tag{6}$$

If $r = 1\,\mu$m, $a = 10$ mm and aluminum wires, the plasma frequency is about 2 GHz and the complex dielectric permittivity is

$$\varepsilon(\omega) = 1 - \frac{\omega_p}{\omega(\omega + j(\varepsilon_0 a^2 \omega_p^2 / \pi r^2 \sigma))} \tag{7}$$

where, for aluminum, $\sigma = 3.65 \times 10^7$ S/m

In Fig. 5a and b is presented the dispersion equations for this structure: the frequency dependency (expressed in plasma frequency units) of real component (Fig. 5a) and imaginary component (Fig. 5b) of the wavenumber.

According to Eq. (7), it can be seen that the wire structure described above has a negative value of the real component of ε up to a value of approximately 0.5 ω_p, after which it became positive taking the asymptotic trend toward 1 for high frequencies. The imaginary component of ε has a maximum for very small values of frequency and after that it will asymptotically decrease toward 0. The dependency of complex dielectric permittivity for the wire structure is presented in Fig. 6a and b.

A specific property of wire-mesh structure is the strong spatial dispersion of the dielectric permittivity, manifested as the formation of TEM modes in addition to the TE and TM modes of an ordinary uniaxial structure [17].

Due to a finite value of the dielectric permittivity of wires, TEM modes acquire hyperbolic dispersion [18]. In this regards, the wire medium represents a particular class of metamaterials with hyperbolic isofrequency surfaces.

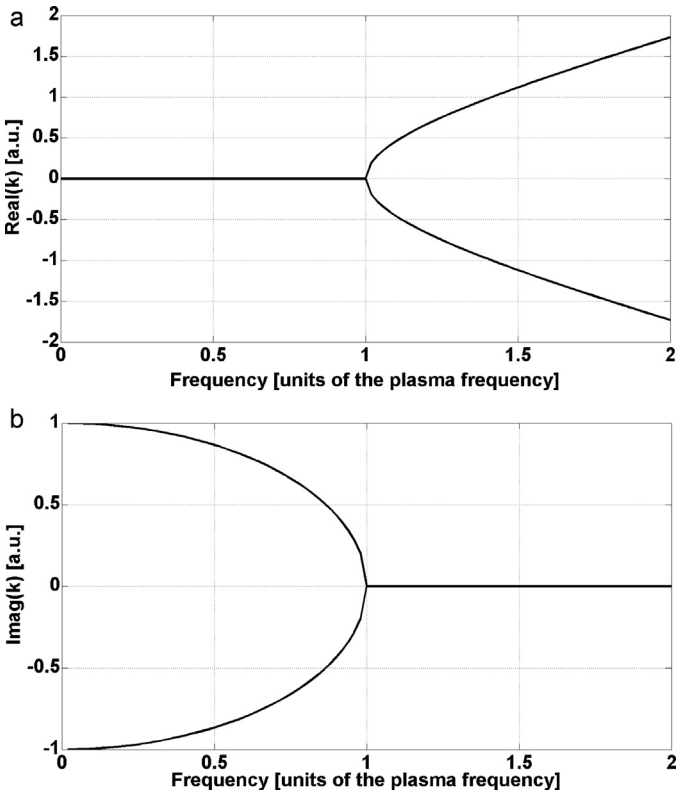

Fig. 5. The dispersion equation for aluminum thin wires of radius 1 μm, and a lattice period of 10 mm, the plasma frequency is about 2 GHz: (a) real part; (b) imaginary part.

2.2. Metamaterial with negative permeability or with positive extremely large permeability

The magnetic activity in most materials tends to fail off at high frequencies of even a few hundred megahertz or a few gigahertz. So it is indeed a challenge even to obtain magnetic activity, let alone negative magnetic permeability, at microwave frequencies and beyond. There are metamaterials which in certain range of frequencies in the above mentioned domain present high positive magnetic permeability, and in other ranges, can have negative magnetic permeability.

From these, only two types extremely used will be presented, namely split ring resonator (SRR) [19–21] and Swiss rolls [2,22,23], with its special variant conical Swiss roll [24].

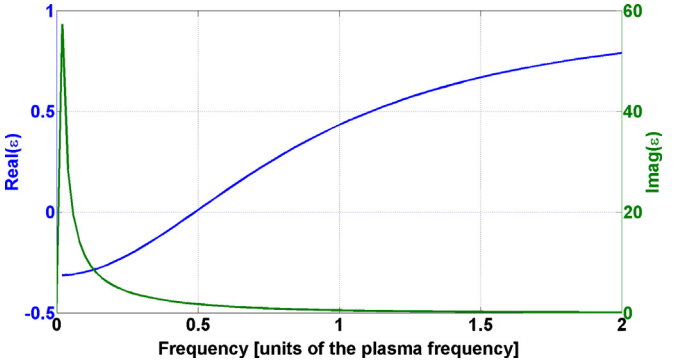

Fig. 6. The dependency by frequency of complex permittivity of aluminum thin wires of radius 1 μm, and a lattice period of 10 mm.

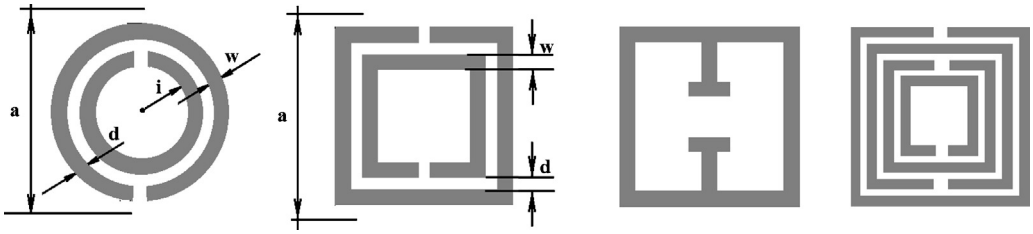

Fig. 7. Split ring resonator: (a) circular structure; (b) squared structure; (c) single ring structure; (d) multiple rings structure.

2.2.1. Split ring resonators

This type of metamaterial has the advantage to be planar, such that its practical realization can be made via photo-lithography for relatively large dimensions and nanolithography for nanometric dimensions, and due this reason, it has been intensively studied. A multitude of variants have been realized, few of them being presented in Fig. 7.

A split ring resonator (SRR) is a highly conductive structure in which the capacitance between the two rings balances its inductance (Fig. 7a). In Fig. 7 b, the circular shape of metallic structure is replaced by a rectangular one of the same structure. In Fig. 7d, multiple split ring resonators are shown, whereas in Fig. 7c other physical realization of SRR is presented.

A time-varying magnetic field applied perpendicularly to the rings surface induces currents which, depending on the resonant properties of the structure, produce a magnetic field that may either oppose or enhance the incident field, thus resulting in positive or negative μ. In other words, the operation of a SRR represents an "over-screened, under-damped" response of metamaterial to electromagnetic stimulation [25].

For a circular double SRR (Fig. 7a), in vacuum and with a negligible thickness of metallic layer, the following approximate expression for μ is valid [19]

$$\mu_{eff} = 1 - \frac{\pi r^2/a^2}{1 + (2\sigma j/\omega r\mu_0) - (3dc^2/\pi^2\omega^2 r^3)} \tag{8}$$

where σ is the metal resistivity and c is the speed of light in vacuum, μ_{eff} has a resonance form presented in Fig. 8.

Examining Fig. 8, the existence of two angular characteristic frequencies, namely the resonance angular frequency of μ_{eff}, ω_0, and "magnetic plasma frequency", ω_{mp}, can be observed. These frequencies can be defined as

$$\omega_0 = \sqrt{\frac{3dc^2}{\pi^2 r^2}}$$
$$\omega_{mp} = \sqrt{\frac{3dc^2}{\pi^2 r^3(1 - (\pi r^2/a^2))}} \tag{9}$$

Below the resonant frequency, μ_{eff} is enhanced, and between ω_0 and ω_{mp}, the real component of μ_{eff} is negative. For a circular SRR with dimensions as mentioned above, $f_0 \cong 0.51$ GHz and $f_{\text{mp}} \cong 1.42$ GHz.

In Fig. 9 is presented the dispersion equation for circular double SRR described above. The two vertical dotted lines correspond to f_0 and f_{mp} frequencies. For $f < f_0$, the circular SRR behavior shows the existence of a transversal mode, followed by a gap between $f_0 < f < f_{\text{mp}}$; for higher frequencies, a longitudinal magnetic plasma mod appears, lacking dispersion.

2.2.2. Swiss roll

A Swiss roll consists of a central cylindrical mandrel, upon which is wound a spiral of conductor with an insulated backing, so that there is no electrical contact between the layers. When an alternating magnetic field is applied along the axis of the cylinder, it induces a current in the conducting sheet. However, the current cannot flow freely, because the sheet is not continuous; it can only flow by virtue of the self-capacitance of the structure which allows the alternative current circuit to be completed [26].

In Fig. 10 is presented the principle scheme of a Swiss roll.

For this type of material, the effective permeability was described in [2]

$$\mu_{eff} = 1 - \frac{F}{1 + (2\sigma i/\omega r\mu_0(N-1)) - (dc^2/2\varepsilon\pi^2 r^3(N-1)\omega^2)} \tag{10}$$

where r is the radius of the mandrel, d is the layer's thickness and N is the number of turns in the spiral. The conductor has a conductivity σ and the insulator between the conductive layers has a permittivity ε. F is the filling factor, the fraction of the material volume which is magnetically active; ideally, this is given as $\pi r^2/a^2$ where a is the lattice spacing. In practice, F is an empirically determined parameter [26].

For the case of Swiss rolls, the resonance frequency f_0 can be defined, as well as for magnetic plasma mode f_{mp}.

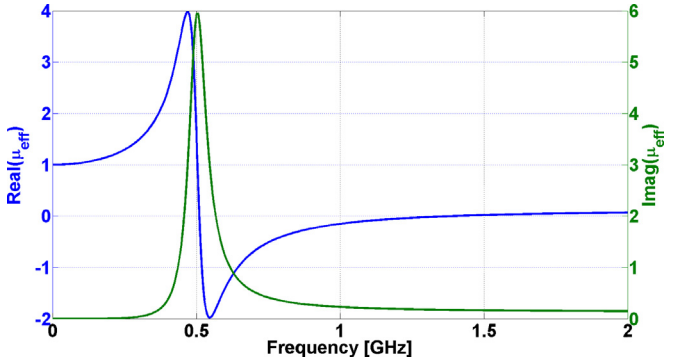

Fig. 8. The effective magnetic permeability for circular double SRR with dimensions: $a = 30$ mm, $r = 16$ mm, $d = 1.5$ mm. $w = 1$ mm, the metal being copper.

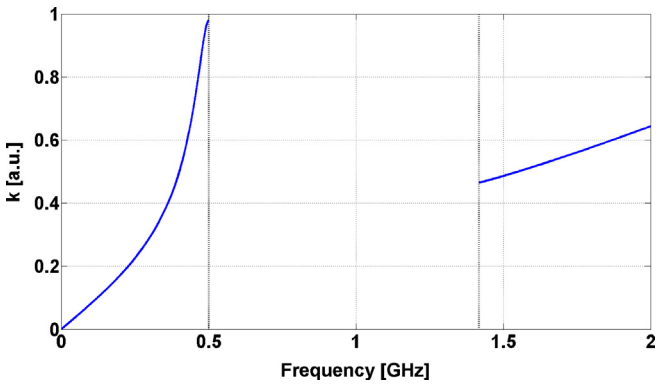

Fig. 9. The dispersion equation for circular double SRR.

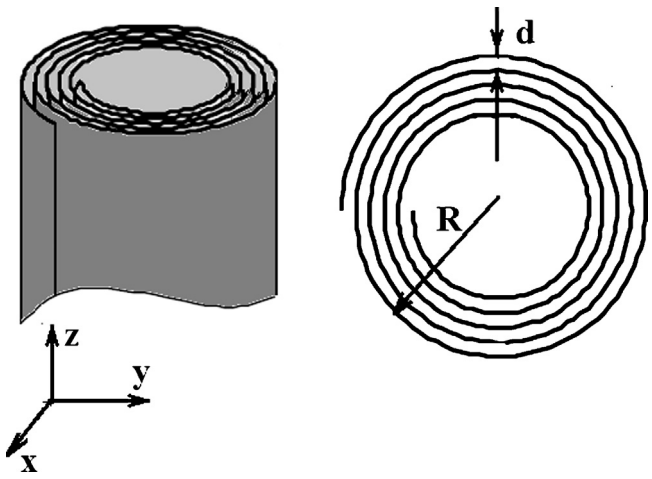

Fig. 10. The principle scheme of a Swiss roll: (a) perspective view; (b) top view.

These frequencies are given by equations [2]

$$f_0 = \frac{1}{4\pi^2}\sqrt{\frac{2dc^2}{r^3(N-1)}}$$
$$f_{mp} = \frac{1}{4\pi^2}\sqrt{\frac{2dc^2}{(1-(\pi r^2/a^2))r^3(N-1)}} \quad (11)$$

Choosing a Swiss roll with $r = 16$ mm, $a = 30$ mm, $d = 0.2$ mm and $N = 1.5$ turns, the dependency of effective permeability by the frequency is presented in Fig. 11.

The values for the resonance frequency and of magnetic plasma mode are $f_0 = 0.622$ GHz and respectively, $f_{mp} = 1.69$ GHz. The dispersion equation can be traced, that, as in case of double circular SRR, presents two-fold degenerate modes, the first at $f < f_0$ and the second at $f > f_{mp}$. For frequencies $f_0 \le f \le f_{mp}$ Swiss roll presents a negative effective permeability, a gap appearing in the dispersion equation, as seen in Fig. 12.

As shown above, it resulted that the metals, good conductive, as well as wire lattices, in a certain frequency range, present $\varepsilon_{eff} < 0$, meanwhile the metamaterials, SRR or Swiss roll types can present $\mu_{eff} < 0$ and by combination, metamaterials with $n < 0$ can be obtained.

The big challenge consists in finding only one metamaterial that presents both $\varepsilon_{eff}, \mu_{eff} < 0$. According to [27,28], such material might be a Swiss roll realized in a special manner, as presented in Fig. 13.

A chiral Swiss roll can be constructed by winding an insulated conducting sheet, with a shape as shown in Fig. 13 (left side), around a cylindrical mandrel, creating an enveloping helix (right side). Each layer of the conductive sheet is separated by a distance d, filled with

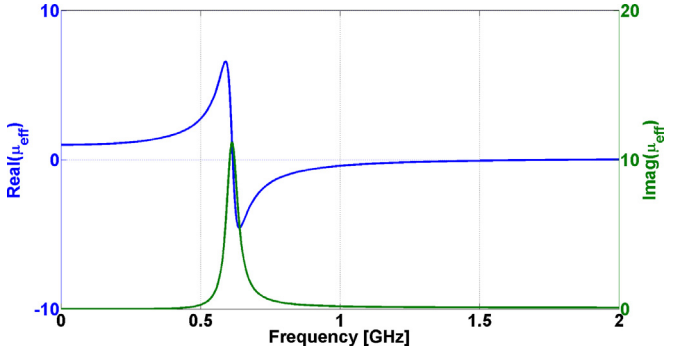

Fig. 11. The dependency of effective permeability by the frequency of a Swiss roll with $r = 16$ mm, $a = 30$ mm, $d = 0.2$ mm and $N = 1.5$ turns.

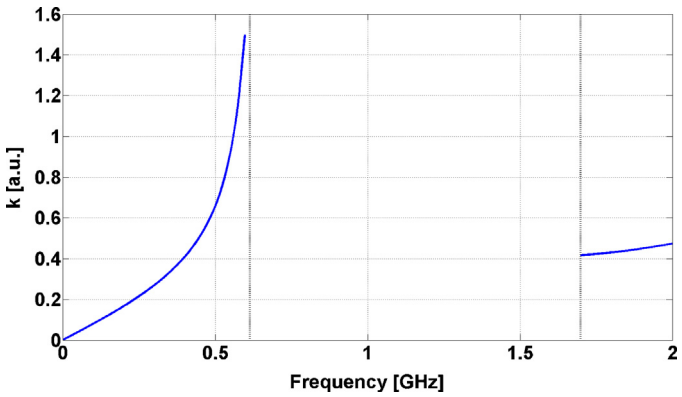

Fig. 12. The dispersion equation for Swiss roll.

a dielectric material of ε_d and N is the number of turns measured on cross section. After [28], resonance frequency is given by

$$f = \frac{c_0}{2\pi}\sqrt{\frac{4\pi Ld\tan^2\theta}{\varepsilon_d(8(N-1)\pi^3R^3\tan^2\theta + a^2d)}} \quad (12)$$

where $L = 1 - \omega(j\varepsilon_d\varepsilon_0 a^2\rho/2\pi R)$, ρ is the resistance of the roll per unit area, R is the external radius of Swiss roll, θ has the significance presented in Fig. 12a. Note that the resistivity losses for microwave frequency are negligible compared to the lossy character of the dielectric in the gap. The magnetic plasma frequency is given by

$$f_{mp} = \frac{f_0}{\sqrt{1-F}} \quad (13)$$

where F is the fill factor $F = (\pi R^2/a^2)$.

For this construction, for frequencies $f_0 < f < f_{mp}$, and a convenient polarized electromagnetic wave, both $\mu_{eff} < 0$ and $\varepsilon_{eff} < 0$ are expected to be obtained.

2.2.3. Conical Swiss roll

When an electromagnetic field with the field vector oriented along the metamaterial axis acts over a Swiss roll, due its high effective magnetic permeability, the field will be guided inside the Swiss roll. This property has been used in [29–31] for the transmission of electromagnetic waves at relatively large distances and with reduced damping. The metamaterials can be used also at the concentration of alternative magnetic fluxes, an example being conical Swiss rolls [24].

A conical Swiss roll consists of a number of spiral-wound layers of an insulated conductor on a conical mandrel, Fig. 14.

The radio frequency magnetic field will induce currents on the circumference of the cone and, consequently, a magnetization opposing the applied magnetic field. The capacitive and inductive elements of the structure create a resonant RLC circuit that the induced currents are subject to. Therefore, a resonant μ that takes high positive, near f_0, and eventually negative values for $f_0 < f < f_{mp}$, as is take place at the Swiss roll described above.

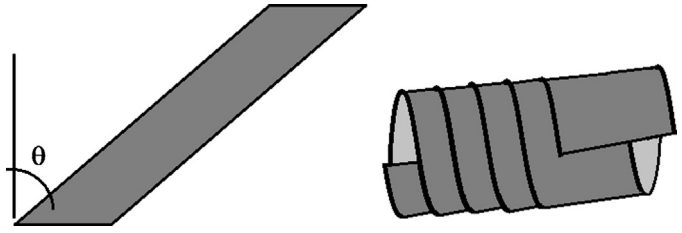

Fig. 13. Chiral Swiss roll: (a) the unfolded conducting sheet used to create a chiral Swiss roll; (b) lateral view.

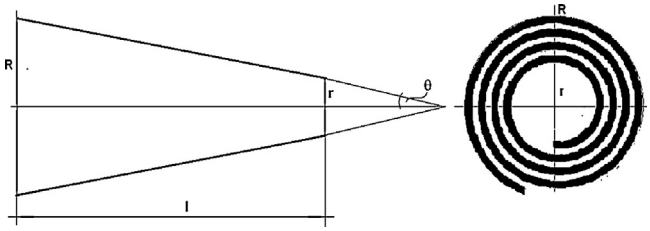

Fig. 14. Conical Swiss roll: (a) lateral view; (b) top view.

For a conical Swiss roll with 5 layers from a copper foil of 18 μm thickness, insulated by a polyamide foil of 12 μm thickness, laminated without adhesive in order to reduce the radiofrequency losses, having 20 mm large base diameter, 3.2 mm small base diameter, 55 mm the height of truncated cone and 20° the aperture of the top angle, the resonance frequency is 72.5 MHz and the effective permeability has the value of 22 [24].

At 4 mm distance from the center of small base of conical Swiss roll, the flux damping is −40 dB reported to the amplitude on the cone axis.

3. Determination of effective constitutive parameters of metamaterials

Considering a periodical structure of metamaterial elements, defined by unit cell of characteristic dimensions a, illuminated by a electromagnetic wave with λ wavelength. The restriction imposed by cell's dimensions is $a \ll \lambda$.

A large value of the wavelength (compared with the lattice dimension) is too myopic to detect internal structure and in this limit an effective permittivity and permeability is a valid concept. In this case, the metamaterial slab behaves as an effective medium. The effective constitutive parameters could be calculated from experimental measurements. As radio and microwave the frequency range is considered here, the most convenient from the experimental point of view is the measurement of S parameters for the metamaterial that fill a waveguide or in free space, using an emission and a reception antennas.

Assuming that the passive metamaterial slab has an effective refractive index n and Z impedance, the effective permittivity ε_{eff} and permeability μ_{eff} are directly calculated from [32]

$$\begin{aligned} \mu_{\text{eff}} &= nZ \\ \varepsilon_{\text{eff}} &= \frac{n}{Z} \end{aligned} \tag{14}$$

The relationship between S parameters and effective refractive index and impedance [21,33] is

$$\begin{aligned} S_{11} &= \frac{U(1-\exp(j2nk_0d))}{1-U^2\exp(j2nk_0d)} \\ S_{21} &= \frac{(1-U^2)\exp(jnk_0d)}{1-U^2\exp(j2nk_0d)} \end{aligned} \tag{15}$$

where $U=(Z-1/Z+1)$

From above equations immediately result

$$\begin{aligned} Z &= \pm\sqrt{\frac{(1+S_{11})^2-S_{21}^2}{(1-S_{11})^2-S_{21}^2}} \\ \exp(jnk_0d) &= W \pm j\sqrt{1-W^2} \end{aligned} \tag{16}$$

where $W=(1/2S_{21}(1-S_{11}^2+S_{21}^2))$.

Since the S parameters are complex, the impedance of the medium and the effective refractive index are also complex, written as $X=X'+jX''$ where X can be Z or n. The signs in Eq. (16) are chosen such that $Z' \geq 0$, $n \geq 0$ because the metamaterial slab is a passive medium [33].

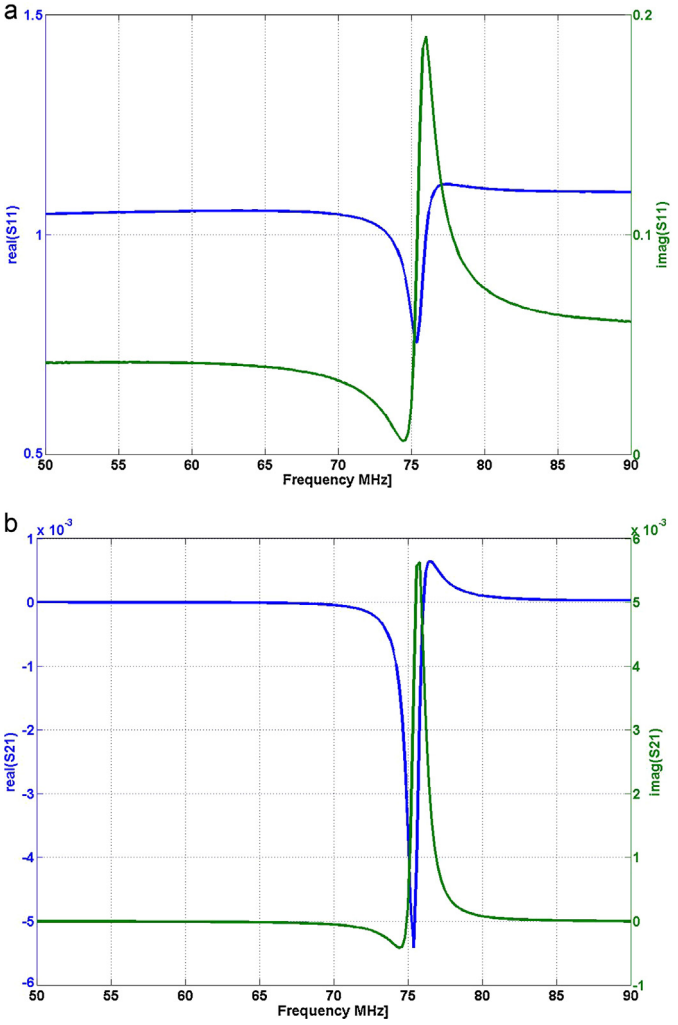

Fig. 15. The dependency by frequency of conical Swiss roll parameters: (a) S_{11}; (b) S_{21}.

Having Z and n determined, the effective permeability and permittivity can be directly calculated.

A method to retrieve the constitutive effective parameters of metamaterials will be explained for the case of conical Swiss roll having 5 layers, 20 mm large base diameter, 3.2 mm small base diameter, 55 mm the height of truncated cone and 20° the aperture of the top angle. The insulated conductor is a copper foil with 18 μm thickness laminated adhesive-less on a polyamide layer with 12 μm thickness (LONGLITE^{TM} 200 produced by Rogers Corporation, USA). The S parameters have been measured using a Network/Impedance/Spectrum Analyzer 4395A Agilent coupled with S Parameters Test kit 87511A Agilent. The incident field is generated by a coil with two turns having 16 mm diameter and a reception coil having two turns of 3 mm diameter [24].

Fig. 15a and b shows the dependency by frequency of S_{11} and S_{21} parameters. Fig. 16 shows the dependency by frequency of effective permeability of a conical Swiss roll with features described above.

Examining the data in Fig. 16 emphasizes the resonant behavior of conical Swiss rolls, both the real component as well as imaginary component of the effective permeability reach maximum value at the same frequency f_0 = 72.5 MHz, namely 22 and respective 16. The frequency range for which the effective permeability is negative is extremely narrow.

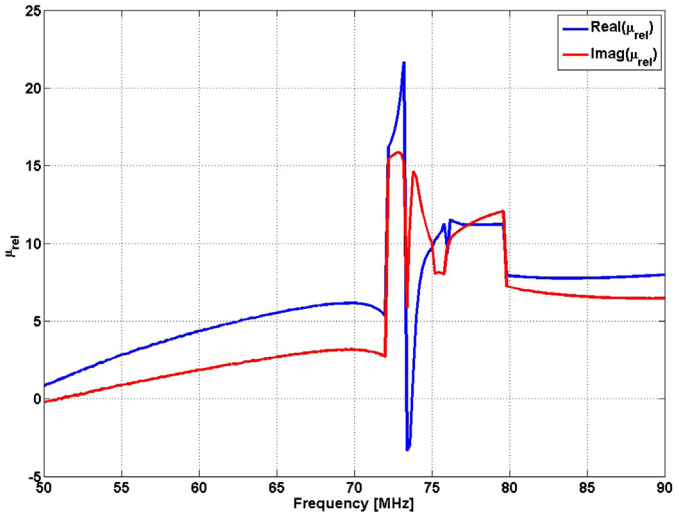

Fig. 16. The frequency dependence of effective permeability of conical Swiss roll.

The effective permittivity and permeability can be determined by measuring reflection and transmission coefficients for normal incidence of the electromagnetic wave to material slab [34], because

$$S_{11} = R$$
$$S_{21} = T\exp(jkd) \tag{17}$$

where R and T are reflection, respective transmission coefficients.

4. Applications of metamaterials

Since the metamaterials properties are so special, their applications are extremely wide. We are focusing on few applications such as perfect lenses, electromagnetic cloaks and different types of nondestructive testing sensors.

4.1. The perfect lens

When ε_{eff} and μ_{eff} of a metamaterials slab have -1 value, simultaneous, the refractive index of the slab is $n = -1$. However, the surface impedance of such as material is given by

$$Z = \sqrt{\frac{\mu_{\text{eff}}}{\varepsilon_{\text{eff}}}} = 1 \tag{18}$$

such that there is no mismatch and hence no reflection at the interface metamaterial slab-air [35]. A slab of this metamaterial not only focusses the electromagnetic field, as shown in [36], but also focusses the evanescent waves as shown in [4].

The plane solution wave for the electric field in vacuum has the form $E_z(r_\parallel, z, t) = E_{z0}\exp[j(k_\parallel r_\parallel + k_z z - \omega t)]$, where $k_{||}$ and k_z are wave numbers along the xy plane and z direction respectively, and they satisfy the dispersion relation as follows $k_\parallel^2 + k_z^2 = (\omega^2/c^2)$ where c is the speed of light in the vacuum.

In the case of $k_\parallel^2 < (\omega^2/c^2)$, k_z is real, corresponding to the propagating wave along the z direction. While $k_\parallel^2 > (\omega^2/c^2)$, k_z is imaginary, corresponding to the evanescent waves along the z direction. The characteristic of the evanescent waves is the exponential attenuation along the propagation direction (Fig. 17).

The loss free metamaterials cannot be made, but with finite loss, imaging with sub-wavelength resolution has been achieved [37].

If the entire experiment is conducted in very near field, the electric and magnetic fields are essentially decoupled, so that a "poor-man's perfect lens" can be made, in which a materials with

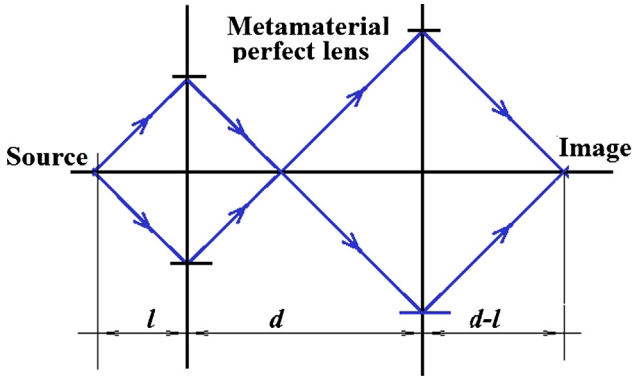

Fig. 17. Perfect lens.

$\varepsilon_{\text{eff}} = -1$ acts on the electric field, or with $\mu_{\text{eff}} = -1$ acts on the magnetic field. These two cases have been demonstrated using silver in the visible spectrum to achieve electric field imaging with $\lambda/6$ resolution [38,39] and using a Swiss roll medium in radiofrequency regime to image magnetic objects with resolution of $\lambda/64$ [30], the maximum resolution being limited by the metamaterials losses according to this simple equation [30]

$$\Delta = \frac{2\pi d}{\left|\ln(\mu''/2)\right|} \tag{19}$$

where d is the slab thickness and $\mu'' = \text{Imag}(\mu_{\text{eff}})$.

In the frequency domain, denoting field quantities by $\bar{E} = \bar{E}(\bar{k}, \omega)$, $\bar{B} = \bar{B}(\bar{k}, \omega)$, etc., the Maxwell curl relations in the absence of free charges yield [40]

$\bar{k} \times \bar{E} = \omega\bar{B}$, $\bar{k} \times \bar{H} = -\omega\bar{D}$, and for linear and homogeneous media, the constitutive relation $\bar{D} = \varepsilon(\omega)\bar{E}$, $\bar{B} = \mu(\omega)\bar{H}$, so that $\bar{k} \times \bar{E} = \omega\mu\bar{H}$, $\bar{k} \times \bar{H} = -\omega\varepsilon\bar{E}$.

If, over a certain frequency range, $\varepsilon(\omega)$ and $\mu(\varepsilon)$ are both real and negative, $\bar{k}$, $\bar{E}$ and $\bar{H}$ form a left-handed triad and the power flow (Poynting vector) $\sim\bar{E} \times \bar{H}$ is antiparallel to $\bar{k}$.

The Snell law at the interface of two dielectric mediums is well-known

$$\frac{\sin\theta_1}{\sin\theta_2} = n_{21} = \left(\frac{\varepsilon_2}{\varepsilon_1}\right)^{1/2} \tag{20}$$

meanwhile, in the case of the two mediums are from metamaterials, or only one it is, the law is written

$$\frac{\sin\theta_1}{\sin\theta_2} = n_{21} = \pm\left(\frac{\varepsilon_{2_{\text{eff}}}\mu_{2_{\text{eff}}}}{\varepsilon_{1_{\text{eff}}}\mu_{1_{\text{eff}}}}\right)^{1/2} \tag{21}$$

In the same time, the reflection coefficient of the electromagnetic wave normal at the interface is characterized by the reflection coefficient

$$r = \frac{n_1 - n_2}{n_1 + n_2} \tag{22}$$

and for the case of metamaterials

$$r = \frac{Z_1 - Z_2}{Z_1 + Z_2} \tag{23}$$

where $Z_1 = (\mu_{1_{\text{eff}}}/\varepsilon_{1_{\text{eff}}})^{1/2}$ and $Z_2 = (\mu_{2_{\text{eff}}}/\varepsilon_{2_{\text{eff}}})^{1/2}$ representing the impedance of the two mediums.

These fundamental equations were first discussed in [41], allowing to anticipate, for materials with negative refractive index, a series of extremely interesting phenomena as anomalous Cerenkov radiation, inverse Doppler effect, etc.

Superlens can be obtained using also hyperbolic metamaterials [42], spatial resolution in the range of $\lambda/60$ being obtained, so over the limit imposed by diffraction.

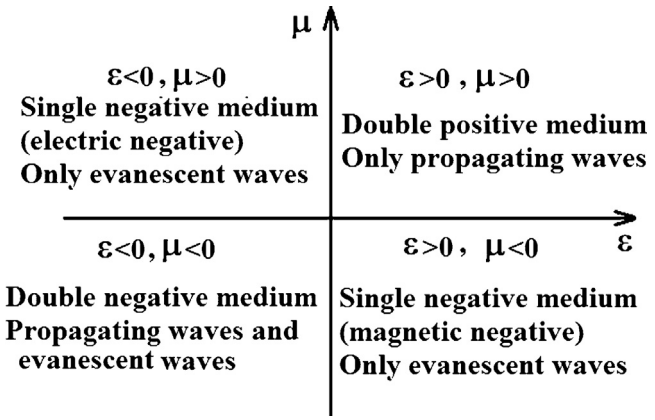

Fig. 18. Schematic representation of materials depending on ε and μ.

The connection between ε and μ for a medium, as well as the wave propagation through it could be schematically represented as in Fig. 18, after [40].

According to the above diagram, a medium having $\mu_{\text{eff}} < 0$ allows the manipulation of evanescent waves, such that, in certain conditions, it should serve for the construction of lens with metamaterials that did not accomplish the conditions imposed for a perfect lens but shall lead to the substantially improvement of the spatial resolution.

Thus, it has appeared the idea of using two conical Swiss roll with the large basis face to face that could operate at a frequency slightly higher than the resonance frequency, as presented in [24].

Let's consider a layout of two Swiss rolls disposed as in Fig. 19. The small basis of the first Swiss roll behaves as a circular aperture and, due to the radio frequency flux concentration properties, previously described; the "rays" that pass inside can be traced.

Thus, the plane "object" is in front of the aperture of Swiss roll I and the focal plane is located in the plane of the small base of Swiss roll II.

In a region without sources, the Helmholtz wave equation is [43]

$$(\nabla^2 + k^2)E(x, y, z) = 0 \tag{24}$$

where k is the wave vector $k = (2\pi f/v)$, with f frequency and v the propagation speed of the electromagnetic waves in the considered media.

In angular representation

$$E(x, y, 0) = \frac{1}{(2\pi)^2}\int_{-\infty}^{+\infty}\int_{-\infty}^{+\infty} E_k(k_x, k_y)e^{j(k_x x + k_y y)}dk_x dk_y \tag{25}$$

where angular spectrum is

$$E_k(k_x, k_y) == \frac{1}{(2\pi)^2}\int_{-\infty}^{+\infty}\int_{-\infty}^{+\infty} E(x', y', 0)e^{-j(k_x x' + k_y y')}dx'dy' \tag{26}$$

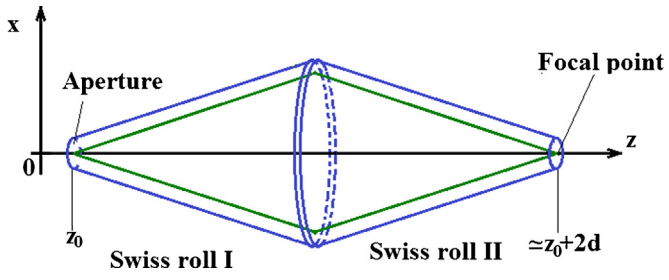

Fig. 19. Layout of two conical Swiss rolls acting as lens to obtain near field images.

If $k^2 > k_x^2 + k_y^2$, the electromagnetic wave is a propagating plane wave, and if $k^2 < k_x^2 + k_y^2$, the electromagnetic wave is an evanescent wave, being rapidly damped along z axis. Consider the propagation nearly parallel to the z axis, (paraxial approximation), such that $E(x, y, z) = E(x, y)e^{jkz}$, situation in which the operation mode of metamaterials lens will be explained using Fourier optics principles [44].

If the evanescent waves are the dominant states, condition met at distances smaller than the wavelength, the field in any z position is

$$E(x, y, z) = \frac{1}{(4\pi)^2}\int_{-\infty}^{+\infty}\int_{-\infty}^{+\infty} f_k(k_x, k_y)e^{jk_x[x+j\text{sign}(k_x)(z-z_0)]+jk_y[y+j\text{sign}(k_y)(z-z_0)]}dk_x dk_y \tag{27}$$

where $f_k(k_x, k_y)$ represents the angular spectrum of the field from aperture

$$\text{sign}(k_x) = \begin{cases} 1 & \text{if} \quad k_x > 0 \\ 0 & \text{if} \quad k_x < 0 \end{cases}$$

$$\text{sign}(k_y) = \begin{cases} 1 & \text{if} \quad k_y > 0 \\ 0 & \text{if} \quad k_y < 0 \end{cases}$$

Considering a wave that has constant angular spectrum in aperture, then truncating the integral from (27) at a double finite sum we obtain

$$f(k_x, k_y) = \begin{cases} E_0 & \text{if} \quad k_a \le k_x \le k_b, k_a \le k_y \le k_b \\ 0 & \text{in} \qquad\qquad \text{rest} \end{cases} \tag{28}$$

Using the Fourier optics method [44]. for the condition given by (28), the field in focal plane is obtained

$$E(x, y, z_0 + 2d) = \frac{E_0}{\pi^2}e^{j((k_b+k_a/2)x+(k_b+k_a/2)y)}\frac{\sin((k_b - k_a/2)x)}{x}\frac{\sin(k_b - k_a/2y)}{y} \tag{29}$$

A relatively uniform angular spectrum can be obtained by scattering an electromagnetic wave on a small scatterer of circular shape made from a material consider as perfect electromagnetic conductor (PEC).

The diameter of a focal spot of the metamaterial lens will be given by [44]

$$D = \frac{4\pi}{k_b - k_a} \tag{30}$$

would be, according to Fig. 19, equal with the diameter of the small basis of the conical Swiss roll, that is 3.2 mm.

Inserting this value in (30), the values of k_b and k_a are obtained, and, the field in the focal plane can be calculated, according to (29).

The verification of this lens functioning has been done using a metallic strip grating having silver strips with 0.6 mm width and 5 μm thickness and slits with 0.4 mm width. Metallic strip grating being illuminated by a TM_z polarized electromagnetic wave, the z axis being orthogonal on the metallic strips plane, only a single pure evanescent mode is induced in slits at excitation frequency of 500 MHz [45]. This mode could be detected and visualized using metamaterials lens described above, the parameters of conical Swiss rolls being presented in [46].

The image of metallic strip grating is obtained and is presented in Fig. 20.

Thus, an approximate λ/2000 spatial resolution can be obtained, the super resolution being achieved due to the possibility to manipulate the evanescent waves.

Lately, in the literature, various variants of perfect lens are presented, promising for possible applications being plasmonic dimple lens, which, at least until now, function at wavelengths in the range of 100 nm [47].

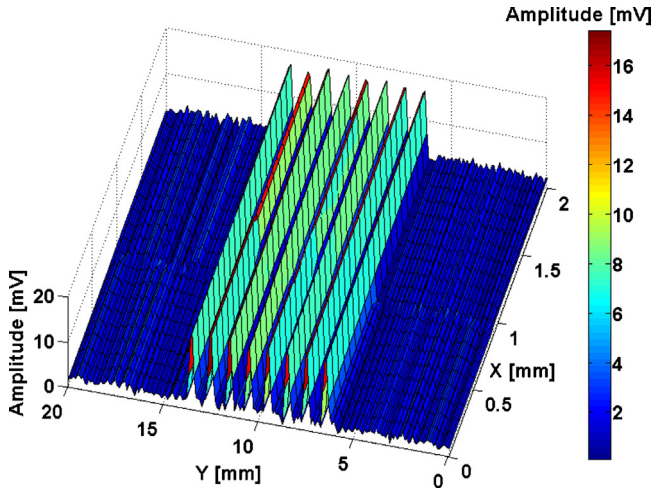

Fig. 20. Electromagnetic image of metallic strip grating using evanescent waves and metamaterials lens.

4.2. Electromagnetic cloak

Recently, a new approach to the design of electromagnetic structures has been introduced, in which the paths of electromagnetic waves are controlled within a material by introducing a prescribed spatial variation in the constitutive parameters [7].

The recipe for determining this variation, based on coordinate transformation, enable us to arrive at structures that would be otherwise difficult to conceive, opening the new field of transformation optics [48].

One possible application of transformation optics and media is that of electromagnetic cloaking in which a material is used to render a volume effectively invisible to incident radiation. Maxwell's equations are form-invariant to coordinate transformations, so that only the components of ε tensor and μ tensor are affected by the transformation, becoming both spatially varying and anisotropic [48]

$$\varepsilon'^{i'j'} = [\det(\Lambda)]^{-1}\Lambda^i_i\Lambda^j_j\varepsilon^{ij}$$
$$\mu' i' j' = [\det(\Lambda)]^{-1}\Lambda^i_i\Lambda^j_j\mu^{ij} \tag{31}$$

where ε and μ are permittivity and permeability, respectively in the original coordinate frame and ε' and μ' are the corresponding quantities in the transformed frame. Λ is given by the first derivative of the coordinate transformation $\Lambda^{j'}_j = (\partial x^{j'}/\partial x^j)$.

We suppose that the object being cloaked is a conductive cylinder of the inner radius of the cloak. The coordinate transformation compresses space from cylindrical region $a < r < b$ into the annular region $a < r' < b$, where r and r' are the radial coordinates on the original and transformed system, respectively a is the cloak inner radius and b is the cloak outer radius. The coordinate transformation is

$$r' = \frac{b-a}{b}r + a, \quad \theta = \theta', \quad z' = z \tag{32}$$

where r, θ, z and r', θ', z' are the cylindrical coordinates in the original system and, respectively, in the transformed system. The transformation given by Eq. (32) impose the following expression for permittivity and permeability tensor components

$$\varepsilon_r = \left(\frac{r-a}{a}\right), \quad \varepsilon_\theta = \mu_\theta = \frac{r}{r-a}, \quad \varepsilon_z = \mu_z = \left(\frac{b}{b-a}\right)^2\frac{r-a}{r} \tag{33}$$

Eq. (33) shows that all the tensor components have gradients as a function of radius. If we suppose that the electric field is polarized along z axis (cylinder's axis) only ε_z, μ_r and μ_θ are relevant components [48]

$$\varepsilon_z = \left(\frac{b}{b-a}\right)^2, \quad \mu_r = \left(\frac{r-a}{a}\right)^2, \quad \mu_\theta = 1 \tag{34}$$

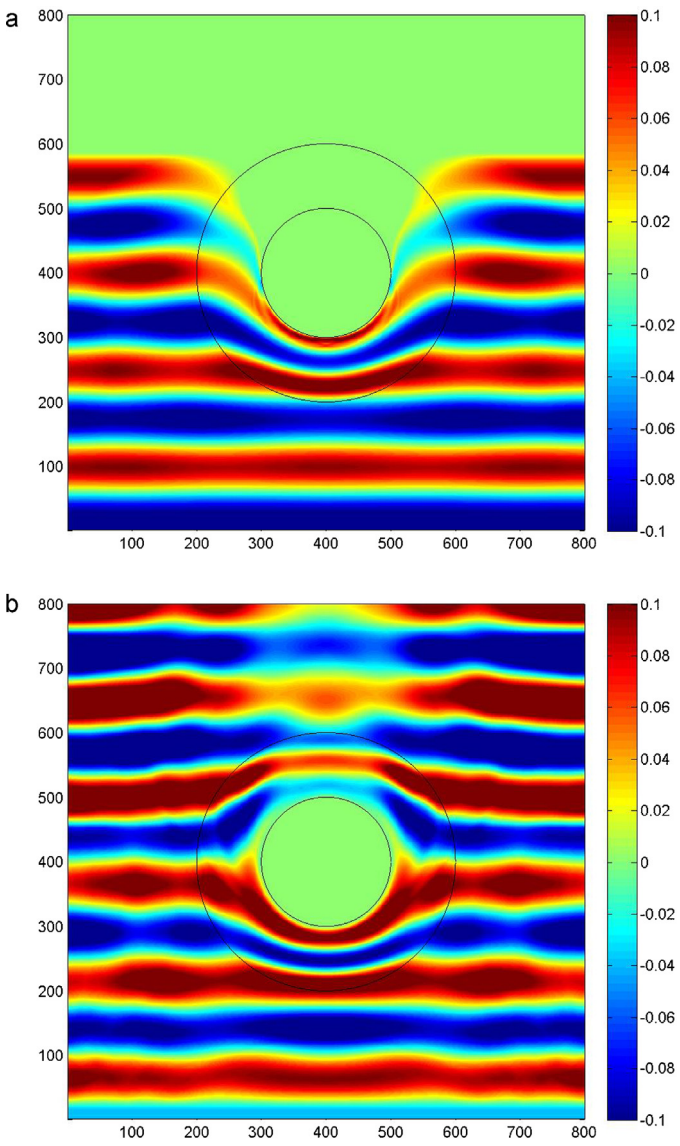

Fig. 21. H_z component of electromagnetic field acting on a cylindrical cloak.

A such medium has been simulated and the possibility to act like a cloak has been studied, for frequency of 2 GHz using a numerical code developed in Matlab based on finite difference time domain (FDTD), starting from the idea presented in [49], for the case $a = 0.1$ mm, $b = 0.2$ mm. The spatial step has been chosen $\Delta x = \Delta y = (\lambda/150)$ and the temporal was $\Delta t = (\Delta x/\sqrt{2}c)$, where c is the speed of light in vacuum. The results are presented in Fig. 21. In Fig. 21a, the H_z field distribution is presented after 800 temporal steps and in Fig. 21b, the same field distribution is presented after 1600 temporal steps.

4.3. Metamaterials sensors for nondestructive evaluation

A large range of sensors is through the possible applications of metamaterials, their functioning and performances depending essentially by the especial properties of metamaterials in the domain of radio frequency and microwave.

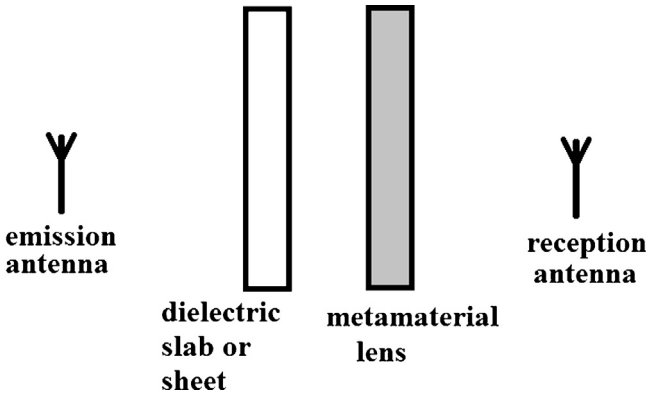

Fig. 22. Schematically representation of dielectric material evaluation.

One of the domains in which these sensors start to be used is nondestructive evaluation (NDE) of materials by electromagnetic procedures.

All researches reported until now, capitalize, in different manners, the possibility to realize perfect lens with metamaterials.

The material to be examined is subdued to the action of an electromagnetic field generated by different types of antennas. For dielectric materials, the most researches [50–53] propose a transmission method for evaluation of material properties and detection of eventually discontinuities, the detection of electromagnetic waves being made after these were propagated through the material to be examined. In order to reach higher performances, between the material to be examined and the reception antenna, a metamaterial lens is inserted, as is schematically presented in Fig. 22.

The best performances obtained in this case consist in the detection of a through hole with 3 mm diameter practiced into a glass fiber reinforced plastic composite plate with $\varepsilon = 4.8$ and 6 mm thickness. The experiments were made at different frequencies and with different types of metamaterial lenses [54–56].

Nondestructive examination applications, in which the information about the material discontinuities is obtained by a reflection method, metamaterial lenses, are also developed [57], the performances of method's sensitivity being comparable with those obtained by transmission.

Also, there are other approaches that allow the substantial improvement of spatial resolution of sensors for electromagnetic

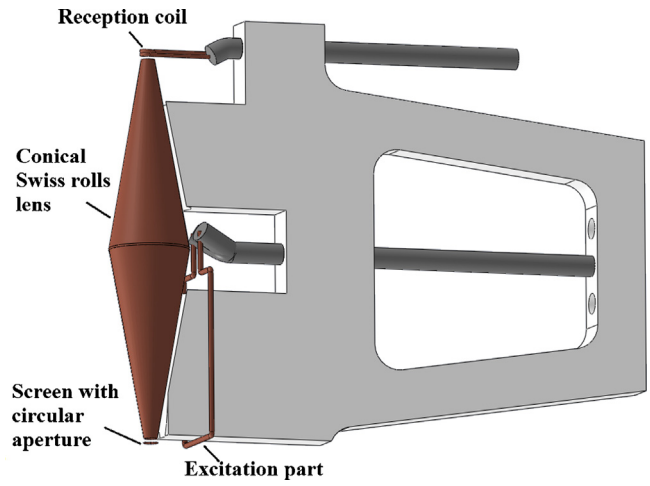

Fig. 23. The layout of metamaterials sensor.

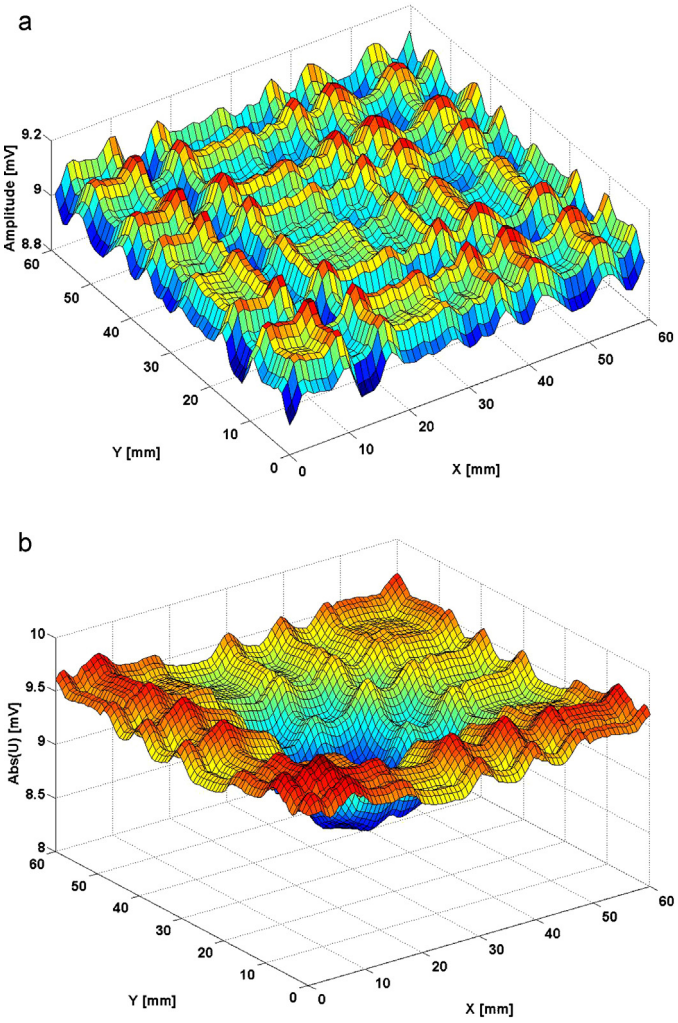

Fig. 24. The measured amplitude of the signal delivered by the electromagnetic transducer with metamaterials from the scanning of a CFRP zone: (a) without delamination; (b) with delamination.

NDE using metamaterials. This method can be used when the defects in composite materials reinforced with long carbon fibers will be detected. The carbon fibers are good electrical conductors and are insulated in composites, one from another, a conductive strip grating being thus created. If this is illuminated with a TM_z polarized electromagnetic wave, in the space between the fibers, filled with a dielectric material, evanescent waves can appear [45,58]. These can be manipulated with a metamaterial lens (described above), detected with a small diameter coil that serves as reception antenna. In order to improve the sensor's spatial resolution, in the focal object plan of the lens is placed a conductive screen having a circular aperture with 0.1 mm diameter [24] (Fig. 23).

In Fig. 24a and b is presented the results obtained with this type of metamaterial sensor at the examination of composite materials having 6 layers of carbon fibers woven type 5 harness satin (Carbon T300 3K 5HS) with a layout that assures the quasi–isotropic properties of the plate were studied. The polymer matrix is made of Polyphenylene Sulphide (PPS). The thickness of the plate is 1.91 mm with a 0.5 volume ratio. The plates are produced by TenCate Advanced Composites, Netherlands.

In Fig. 24a, the carbon fibers from the woven are clearly visible meanwhile in Fig. 24b, a delamination due to an impact with low energy (2.5J) became visible.

5. Conclusions

The theoretical and experimental study of electromagnetic metamaterials gained in the last 20 years, a special development. These media have special properties such as negative permittivity and very high or negative magnetic permeability in the range of radio and microwave frequencies and, also, the metamaterials which are lossless within a narrow frequency range. These properties are dependent on the selection of structural elements types, geometrical dimensions, and the dimensions of unit cell as well as the operation frequency. Currently, there is a wide range of structural elements. A special attention is granted to conical Swiss rolls which, exhibit both high and negative permeability and also concentrate the magnetic flux in the domain of radio and microwave frequency, without being perturbed by a continuum intense magnetic field. The constitutive parameters of metamaterials can be extracted from S parameters or reflection and transmission coefficients measurements. The possibilities to use metamaterials are very numerous, with many researchers focusing on the possibility of realization of perfect lens and lenses with metamaterials with negative permeability that allow the manipulation of evanescent waves. Electromagnetic cloak can be simulated, in present, and also realized, even if the electromagnetic "invisibility" is assured for a narrow band of frequencies. Other application is the realization of new types of sensors for nondestructive evaluation of materials by electromagnetic procedures. The sensor based on a lens with conical Swiss rolls that allows the manipulation of evanescent waves can reach a spatial resolution of $\lambda/2000$ and can be used for the examination of carbon fiber reinforces plastics composites for visualization of carbon fibers layout and delaminations.

Acknowledgements

This paper is partially supported by the Romanian Ministry of Education, Research and Innovation under Nucleus Program – Contract no. 09 43 01 04 and Bilateral Cooperation Project 468/2011 MENDE Ro-Sk/2011.

References

[1] M. Lapine, S. Tretyakov, IET Microwaves, Antennas and Propagation 1 (2007) 3–11.
[2] J.B. Pendry, A.J. Holden, D.J. Robbins, W.J. Stewart, IEEE Transactions on Microwave Theory and Techniques 47 (1999) 2075–2096.
[3] A. Shivola, in: A. Shivola (Ed.), Advances in Electromagnetic of Complex Media and Metamaterials, Kluver, Dordrecht, 2003, pp. 1–17.
[4] J.B. Pendry, Physical Review Letters 85 (2000) 3966–3969.
[5] V.A. Pololskiy, N.A. Kuhta, G.W. Milton, Applied Physics Letters 87 (2005) 231113.
[6] M.W. Feise, Y.S. Kivshar, Physics Letters A 324 (2005) 326–330.
[7] D. Schurig, J.J. Mock, B.J. Justice, S.A. Cummer, J.B. Pendry, A.F. Starr, D.R. Smith, Science 314 (2006) 977–980.
[8] W. Cai, V.K. Chettiar, A.V. Kildishev, V.M. Sholoev, Nature Photonics 1 (2007).
[9] E. Lier, R.K. Show, Electronics Letters 44 (2008) 1444–1445.
[10] E. Lier, D.H. Werner, C.P. Scarborough, Q. Wu, J.A. Bossard, Nature Materials 10 (2011) 216–222.
[11] A. Alu, N. Engheta, Physical Review B 78 (2008) 1098–1121.
[12] J.H. Lee, J.G. Yook, Applied Physics Letters 92 (2008) 254103.
[13] J. Zaran, O. Jaksic, C. Kment, Journal of Optics A-Pure and Applied Optics 9 (2007) 377–384.
[14] J.B. Pendry, A.J. Holden, W.J. Stewart, I. Youngs, Physical Review Letters 76 (1996) 4773–4776.
[15] H. Rother, Surface Plasmons on Smooth and Rough Surfaces and on Gratings, Springer-Verlag, New York, 1988.
[16] L.D. Landau, E.M. Lifshitz, The Classical Theory of Fields, vol. 2, 4th ed., Butterworth-Heinemann, 1975.
[17] P.A. Belov, R. Marques, S.I. Maslovski, I.S. Nefedov, M. Silveirinha, C.R. Simovski, S.A. Tretyakov, Physical Review B 67 (2003) 113103.
[18] M. Silveirinha, Physical Review E 73 (2006) 046612.
[19] D.R. Smith, W.J. Padilla, D.C. Vier, S.C. Nemat-Nasser, S. Schultz, Physical Review Letters 84 (2000) 8184–8187.
[20] A. Shelby, D.R. Smith, S. Schultz, Science 292 (2001) 77–79.
[21] R.A. Shelby, D.R. Smith, S.C.Nemat Nasser, S. Schultz, Applied Physics Letters 78 (2011) 489–491.
[22] A. Demetriadou, J.B. Pendry, Journal of Physics: Condensed Matter 21 (2009) 326006.
[23] M.C.K. Wiltshire, Physica Status Solidi 244 (2007) 1227–1236.
[24] R. Grimberg, A. Savin, R. Steigmann, B. Serghiac, A. Bruma, INSIGHT 53 (3) (2011) 132–137.
[25] S. Ramakrishna, Reports on Progress in Physics 68 (2005) 449–521.
[26] M.C.K. Wiltshire, J.B. Pendry, I.R. Young, D.J. Larkman, D.J. Gilderdale, J.V. Hajnal, Science 291 (2001) 849–851.
[27] A. A.Demetriadou, J.B. Pendry, Physica B-Condensed Matter 405 (2010) 2943–2946.
[28] A. A.Demetriadou, J.B. Pendry, Journal of Physics: Condensed Matter 21 (2009) 376003.
[29] M.C.K. Wiltshire, J.V. Hajnal, J.B. Pendry, D.J. Edwards, C.J. Stevens, Optic Express 11 (2003) 709–715.
[30] M.C.K. Wiltshire, J.B. Pendry, J.V. Hajnal, Journal of Physics: Condensed Matter 18 (2006) 315–328.
[31] M.C.K. Wiltshire, J.B. Pendry, W. Williams, J.V. Hajnal, Journal of Physics: Condensed Matter 19 (2007) 456216.
[32] J.A. Kong, Electromagnetic Wave Theory, EMW, Cambridge, MA, 2000.
[33] X. Chen, T.M. Grzegorczyk, B.-I. Wu, J. Pacheco, J.A. Kong, Physical Review E 70 (2004), 016608, 1-7.
[34] D.R. Smith, S. Schultz, P. Markoš, C.M. Soukoulis, Physical Review B 65 (2002) 195104.
[35] D.R. Smith, J.B. Pendry, M.C.K. Wiltshire, Science 305 (2004) 788–792.
[36] V.G. Veselago, Soviet Physics Uspekhi 10 (1968) 509–514.
[37] A. Grbic, G.V. Eleftheriades, Physical Review Letters 92 (2004) 117402.
[38] R.J. Blaikie, D.O. Melville, Journal of Optics A-Pure and Applied Optics 7 (2005) S176–S183.
[39] N. Fang, H. Lee, C. Sun, X. Zhang, Science 308 (2005) 534–537.
[40] M.W.Mc Call, Journal of Modern Optics 56 (2009) 1727–1740.
[41] V. Veselago, L. Braginsky, V. Shklover, C. Hafner, Journal of Computational and Theoretical Nanoscience 3 (2006) 1–30.
[42] F. Lemoult, M. Fink, G. Lerosey, Nature Communications 3 (2012) 889.
[43] J. Van Bladel, Electromagnetic fields, 2nd ed., IEEE Press, Hoboken, NJ, 2007.
[44] M. Born, E. Wolf, Principles of Optics, 7th ed., Cambridge University Press, Cambridge, 2002.
[45] R. Grimberg, G.Y. Tian, Proceedings of the Royal Society A 468 (2012) 3080–3099.
[46] R. Grimberg, A. Savin, R. Steigmann, NDT & E International 46 (2012) 70–76.
[47] S. Vedantam, H. Lee, J. Tang, J. Conway, M. Staffaroni, E. Yablonovitch, Nano Letters 9 (2009) 3447–3452.
[48] J.B. Pendry, A. Aubry, D.R. Smith, S.A. Maier, Science 327 (2012) 549–552.
[49] V.E. Elander, Mathematical modeling of metamaterials, Ph.D. Thesis, University of Nevada, Las Vegas, 2011.
[50] M. Tabib-Azar, D.-P. Su, A. Pohar, S.R. LeClair, G. Ponchak, Review of Scientific Instruments 70 (1999) 1725–1729.
[51] S.I. Ganchev, N. Qaddoumi, S. Bakhtiari, R. Zoughi, IEEE Transactions on Instrumentation and Measurement (1995) 1023–1029.
[52] M.S. Boybay, O.M. Ramahi, Physical Review E 79 (2009) 016602.
[53] K. Aydin, I. Bulu, E. Ozbay, Applied Physics Letters 90 (2007) 254102.
[54] K. Aydin, I. Bulu, E. Ozbay, Optics Express 13 (2005) 8753–8759.
[55] D. Shreiber, M. Gupta, R. Cravey, Microwave nondestructive evaluation of dielectric materials with a metamaterial. Lens, NASA Rep. 20080043, 2006.
[56] D. Shreiber, M. Gupta, R. Cravey, Sensors and Actuators A: Physical 165 (2011) 256–260.
[57] Y. Deng, X. Liu, Sensors 11 (2011) 11774–11808.
[58] R.Grimberg, A. Savin, Electromagnetic transducer for evaluation of structure and integrity of the composite materials with polymer matrix reinforced with carbon fibers, Patent RO126245-A0/2011.